

Manipulating Majorana zero modes in the spin-1/2 Kitaev ladder

Haoting Xu¹ and Hae-Young Kee^{1,2,*}

¹*Department of Physics, University of Toronto, 60 St. George St., Toronto, Ontario, Canada M5S 1A7*

²*Canadian Institute for Advanced Research, CIFAR Program in Quantum Materials, Toronto, Ontario, Canada M5G 1M1*

(Dated: April 26, 2024)

The one-dimensional p -wave superconductor, characterized by boundary Majorana modes, has attracted significant interest owing to its potential application in topological quantum computation. Similarly, spin-1/2 Kitaev ladder systems with bond-dependent Ising interactions, featuring Majorana fermions coupled with Z_2 flux, exhibit boundary Majorana modes when in a topological phase. However, the ground state degeneracy, inherent in these systems, may result in the annihilation of Majorana modes due to the superposition of the two states. To address this issue, we introduce a projective measurement that selects one of the degenerate Z_2 sectors, enabling the emergence of Majorana modes. Once the state is selected, we show that the application of the local spin operators on a bond flips the sign of the adjacent Z_2 flux. Repeating such operators enables the system to reach a desired Z_2 flux configuration. We present the phase diagram and the appearance of Majorana modes at the interfaces of topological and non-topological phases. These modes, along with boundary Majorana modes, can be manipulated and fused by tuning the flux sectors achievable through applying local spin operators. We also discuss the engineering of the Kitaev ladder and open questions for future studies.

I. INTRODUCTION

Decoherence of quantum states is recognized as one of the most serious challenges to realizing quantum computers. Topological quantum computation (TQC) provides an elegant solution to the decoherence issue by storing and manipulating quantum information non-locally in the topological qubits [1–6]. The topological qubits are based on fractionalized excitations of many-body systems with long-range entanglement, which encode non-Abelian statistics.

Searching for material platforms to realize fractionalized excitations has been one of the central themes in condensed matter physics. Examples of such platforms include chiral $p + ip$ superconductors. Within the vortex core of these chiral $p + ip$ superconductors, the emergence of Majorana zero modes, zero energy bound states, is facilitated by the additional angular momentum arising from the superconducting pairing.[7] Subsequently, it was demonstrated that half-quantum vortices, constituting half of a single vortex, harboring Majorana fermions within chiral p -wave superconductors exhibit non-Abelian statistics.[8] Due to the challenges of finding the chiral p -wave bulk materials, proposals have been made to engineer chiral p -wave superconductors by leveraging the proximity effect of spin-orbit coupling in conventional superconductors.[9]

An alternative approach has also been developed. Quantum spin liquids in frustrated magnetic systems offer fractionalized excitations. Among them, the Kitaev spin model composed of the bond-dependent Ising interaction exhibits the Majorana fermions and Z_2 vortices which obey the non-Abelian statistics under the magnetic

field. [10] While there is a growing list of the spin-1/2 Kitaev candidate materials, including honeycomb Na_2IrO_3 , $\alpha\text{-RuCl}_3$, and cobaltates[11–20], the quest for a definite example of quantum spin liquids remains unresolved.

Parallel to the search for two-dimensional (2D) candidate materials, research also focuses on one-dimensional (1D) topological systems. In particular, the p -wave topological superconductor, which hosts edge Majorana zero modes, has been extensively studied. [21–29] It was demonstrated that the Majorana zero modes fuse to vacuum and fermion sector [27, 30–32], and the Majorana fermions encode non-Abelian statistics when forming a wire network [31]. It was shown that the braiding of Majorana fermions can be conducted with a minimum of T-junction geometry and the fusion of Majorana fermions may be detected through a parity-to-charge conversion[30, 31, 33]. In these setups, one significant ingredient is to change the topological nature of the wire, which may be realized through external voltage to change the chemical potential of the electrons[31].

Motivated by research into 1D p -wave superconductivity and the Kitaev honeycomb model, we investigate the 1D version of the Kitaev honeycomb model, the spin-1/2 Kitaev ladder, as illustrated in Fig. 1, where x , y , and z refer to the spin-1/2 Ising interaction of the form $S_i^\gamma S_j^\gamma$ with $\gamma = x, y, z$. This model is exactly solvable using the Jordan-Wigner transformation, which effectively maps the spin-1/2 system to fermionic systems through a non-local transformation.[34–36] Furthermore, it has been demonstrated that the anisotropic Kitaev ladder phase exhibits a symmetry-protected topological phase characterized by a string order parameter.[37–42] The Kitaev phase can be conceptualized as a pair of Majorana fermions coupled to a Z_2 flux defined on a bond (or equivalently square plaquette). The two degenerate ground states under periodic boundary conditions (PBC) are connected by the Z_2 flux transformation. Conse-

* hy.kee@utoronto.ca

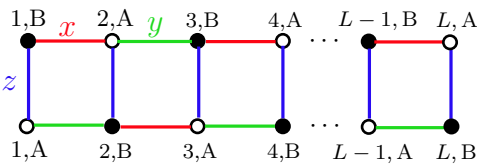


Fig. 1. The Kitaev ladder with bond-dependent nearest neighbour Ising interaction. The red, green and blue bonds indicates x, y and z bond respectively.

quently, if an arbitrary superposition of the two degenerate ground states is considered, the Majorana fermions from the two Z_2 flux configurations may annihilate or form complex fermions. However, by selectively choosing a specific Z_2 flux sector through projective measurement, a single Majorana fermion emerges at each end of the open boundary, which can be further controlled by manipulating the Z_2 flux. Here we propose how to select a desired Z_2 flux configuration and control the Majorana fermions.

The paper is organized as follows. In Sec. II, we first review how the model can be written as Majorana fermion coupled with Z_2 flux, which is defined on a bond, by Jordan-Wigner transformation. We then demonstrate how to select a fixed configuration of the Z_2 flux among the two degenerate states. In Sec. III, we present the phase diagram of the π -flux, which is the ground state, of the anisotropic Kitaev ladder and identify different topological phases. We then investigate the phase diagram with 0-flux sector. In Sec. IV, we perform analytical and numerical analysis to demonstrate the emergent Majorana fermion modes at the boundary or interface between topological and non-topological phases. In Sec. V, we demonstrate that the Majorana modes can be moved and fused by changing the flux via applying local spin operators. In Sec. VI, we discuss the engineering the Kitaev ladder out of the honeycomb structure by replacing $J_{\text{eff}} = 1/2$ ions with a nonmagnetic ions except for the two zig-zag chains. The shape of the ladder, consisting of two coupled zig-zag chains, differs from the regular ladder due to an alternating bond length between the chains. The phase diagram of the modified Kitaev interaction is presented. In Sec. VII, we summarize our results and discuss open questions for future studies.

II. PREPARING A SPECIFIC Z_2 FLUX SECTOR IN THE KITAEV LADDER MODEL

In this section, we discuss the method to prepare and tune the configurations of the Z_2 flux. First, we review the Jordan-Wigner transformation which transforms the spin system into the fermion system.

We consider a spin- $\frac{1}{2}$ ladder with bond-dependent Ising interaction with L unit cells, corresponding to $N = 2L$ sites in total, as depicted in Fig. 1. The Hamiltonian of

the system is given by

$$\mathcal{H} = \sum_{j=1}^L \frac{1}{4} (K_x \sigma_{j,B}^x \sigma_{j+1,A}^x + K_y \sigma_{j,A}^y \sigma_{j+1,B}^y + K_z \sigma_{j,A}^z \sigma_{j,B}^z), \quad (1)$$

where $\sigma_{j,\mu}$ are the Pauli matrices on each site and $\mu = (A, B)$ is the sublattice index. To represent the Hamiltonian, \mathcal{H} , in terms of Majorana fermion, we map the spin system to a fermion system using Jordan-Wigner transformation. The Jordan-Wigner fermion is defined by $f_{j,\mu}^\dagger = \sigma_{j,\mu}^+ S(j, \mu)$, where the string operator, $S(j, \mu)$, is defined by

$$S(j, \mu) = \begin{cases} \prod_{\substack{k < j \\ (k, \nu) \in \mathcal{L}_B}} \sigma_{k, \nu}^z, & (j, \mu) \in \mathcal{L}_B, \\ \prod_{\substack{k < j \\ (k, \nu) \in \mathcal{L}_T}} \sigma_{k, \nu}^z \prod_{(l, \alpha) \in \mathcal{L}_B} \sigma_{l, \alpha}, & (j, \mu) \in \mathcal{L}_T, \end{cases} \quad (2)$$

where \mathcal{L}_B and \mathcal{L}_T represents the set of spins at the bottom ladder and the top ladder, respectively. Majorana fermions are defined as

$$\begin{aligned} \gamma_{j,A} &= f_{j,A} + f_{j,A}^\dagger, & \tilde{\gamma}_{j,A} &= i(f_{j,A}^\dagger - f_{j,A}), \\ \gamma_{j,B} &= i(f_{j,B}^\dagger - f_{j,B}), & \tilde{\gamma}_{j,B} &= f_{j,B} + f_{j,B}^\dagger, \end{aligned} \quad (3)$$

where they satisfy $\{\gamma_{j,\mu}, \gamma_{k,\nu}\} = 2\delta_{jk}\delta_{\mu\nu}\mathbb{1}$, $\{\tilde{\gamma}_{j,\mu}, \tilde{\gamma}_{k,\nu}\} = 2\delta_{jk}\delta_{\mu\nu}\mathbb{1}$, and $\{\gamma_{j,\mu}, \tilde{\gamma}_{k,\nu}\} = 0$. According to the definition in Eq. 3, each complex f -fermion is represented by two Majorana fermions, thereby preserving the size of the Hilbert space. Consequently, the Kitaev Hamiltonian, \mathcal{H} , is represented by

$$\mathcal{H} = \sum_j \left[\frac{K_x}{4} i\gamma_{j,B}\gamma_{j+1,A} - \frac{K_y}{4} i\gamma_{j,A}\gamma_{j+1,B} + \frac{K_z}{4} (i\gamma_{j,A}\gamma_{j,B})(i\tilde{\gamma}_{j,A}\tilde{\gamma}_{j,B}) \right]. \quad (4)$$

We define a Z_2 flux on the vertical bond, D_j , as $D_j = i\tilde{\gamma}_{j,A}\tilde{\gamma}_{j,B}$, which commutes with the Hamiltonian and each other. Hence the Hamiltonian, \mathcal{H} , can be diagonalized in different $\{D_j\}$ sectors. D_j can take values of either $+1$ or -1 . Specifically, the ground state of the ladder stays in the π -flux sector, defined by $D_j D_{j+1} = -1$, according to the Lieb's theorem[43]. This means that the ground state has the $\{D_j\}$ configuration of either $\{D_j\} = \{+1, -1, \dots\}$ or $\{D_j\} = \{-1, +1, \dots\}$. The sector $\{D_j\}$ and the sector $\{-D_j\}$ have the same energy spectrum for Majorana fermions. This is because the transformation $D_j \rightarrow -D_j$ for all j is equivalent to $\gamma_{j,\mu} \rightarrow -\gamma_{j,\mu}$ for $(j, \mu) \in \mathcal{L}_B$. Such a local phase factor added to the definition of Majorana fermions does not change the energy spectrum. Hence, when considering PBC, the model contains a double degeneracy, due to the equivalence of Majorana fermion spectrum for $\{D_j\}$ and $\{-D_j\}$ sectors, i.e., $\{D_j\} = \{+1, -1, \dots\}$ and $\{D_j\} = \{-1, +1, \dots\}$.

In order to see the edge Majorana mode in the topological phase, the double degeneracy must be broken by choosing a specific flux sector. This can be done by applying projective measurement to select the desired $\{D_j\}$ sector, which corresponds to non-local spin operations. In spin representation, D_j takes the form of

$$D_j = \begin{cases} \sigma_{j,A}^x \sigma_{j,B}^x \prod_{\substack{k>j \\ (k,\mu) \in \mathcal{L}_B}} \sigma_{k,\mu}^z \prod_{\substack{l<j \\ (l,\nu) \in \mathcal{L}_T}} \sigma_{l,\nu}^z, & j \text{ is odd,} \\ -\sigma_{j,A}^y \sigma_{j,B}^y \prod_{\substack{k>j \\ (k,\mu) \in \mathcal{L}_B}} \sigma_{k,\mu}^z \prod_{\substack{l<j \\ (l,\nu) \in \mathcal{L}_T}} \sigma_{l,\nu}^z, & j \text{ is even.} \end{cases} \quad (5)$$

The preparation of a specific flux sector can be achieved by projective quantum measurement of D_j on a single bond. Consider any linear combination of the ground state, $|\psi\rangle = \psi_1| \{+1, -1, \dots\} \rangle + \psi_2| \{-1, +1, \dots\} \rangle$. After applying the projector, $\Pi_1^+ = (1 + D_1)/2$, the quantum state becomes $\Pi_1^+|\psi\rangle = | \{+1, -1, \dots\} \rangle$. Similarly, after applying the projector, $\Pi_1^- = (1 - D_1)/2$, the quantum state becomes $\Pi_1^-|\psi\rangle = | \{-1, +1, \dots\} \rangle$.

After the preparation of the specific Z_2 flux sector, the Z_2 flux can be manipulated by applying local spin operators. The local spin operators that flip the sign of D_j and D_{j+1} are

$$U_{(j,j+1)} = \sigma_{j,A}^x \sigma_{j+1,B}^x = i\tilde{\gamma}_{j,A} \tilde{\gamma}_{j+1,B}, \quad (6)$$

which are nearest-neighbor spin operators. It is straight forward to check that

$$U_{(j,j+1)} D_l U_{(j,j+1)}^\dagger = -D_l (\delta_{l,j} + \delta_{l,j+1}), \quad (7)$$

which means that the operation $U_{j,j+1}$ flips the sign of D_j and D_{j+1} . The unitary operator can also be $\sigma_{j,B}^y \sigma_{j+1,A}^y = -i\tilde{\gamma}_{j,B} \tilde{\gamma}_{j+1,A}$, which flips the sign of D_j and D_{j+1} as well. Hence, any configuration of $\{D_j\}$ can be reached by applying projective quantum measurement and local spin operators. A potential realization of applying local spin operators on the spin systems is discussed in Appendix B.

III. PHASE DIAGRAM OF KITAEV LADDER

In order to obtain the phase diagram of the Kitaev spin ladder for a given flux sector, we exactly solve the Majorana hopping problem for given $\{D_j\}$ with PBC. The π -flux sector, also denoted as the ground state sector, satisfies $D_j D_{j+1} = -1$. Flux excitations with other $\{D_j\}$ configurations are gapped. In π -flux sector, there are four bands in the dispersion, corresponding to the four sublattices. The energy dispersion of the four bands takes the form of $(\epsilon_{k,+}^\pi, \epsilon_{k,-}^\pi, -\epsilon_{k,+}^\pi, -\epsilon_{k,-}^\pi)$, where

$$\epsilon_{k,\pm}^\pi = \frac{1}{2} \sqrt{(K_z \pm (K_x - K_y) \sin \frac{k}{2})^2 + (K_x + K_y)^2 \cos^2 \frac{k}{2}}. \quad (8)$$

The energy gap closes at $|K_x - K_y| = K_z$, indicating a topological phase transition at these lines. The phase transition lines and the phases for the ground state sector are depicted in Fig. 2, where T_x and T_y denote two topological phases, NT denotes the non-topological phase. The existence of edge modes can be observed at extreme parameter limits and maintained within the same phase without closing the energy gap. For the T_x phase, one can consider the limit where $K_x \gg K_y, K_z$. In this limit, the Majorana fermions on each x -bond are coupled, leaving one Majorana fermion on the left and right edges as the edge Majorana modes. For the NT phase, one consider the limit where $K_z \gg K_x, K_y$. This configuration leads to the coupling of Majorana fermions across each rung, resulting in the absence of edge modes, in contrast to the T_x phase. To see the relation between Majorana fermions and spins, we solve the limit $K_z \gg K_x, K_y$ using perturbation theory in Appendix A.

For 0-flux sector, i.e., $\{D_j\} = \{+1, +1, \dots\}$ or $\{D_j\} = \{-1, -1, \dots\}$, the fermion bands are $(\epsilon_{k,+}^0, \epsilon_{k,-}^0, -\epsilon_{k,+}^0, -\epsilon_{k,-}^0)$, where

$$\epsilon_{k,\pm}^0 = \frac{1}{2} \sqrt{(K_z \pm (K_x + K_y) \cos \frac{k}{2})^2 + (K_x - K_y)^2 \sin^2 \frac{k}{2}}. \quad (9)$$

Here, the transition lines are $|K_x + K_y| = K_z$ and $K_x = K_y$ with $(|K_x + K_y| > K_z)$. The phase diagram and the corresponding $\{D_j\}$ configurations for the 0-flux sector are illustrated in Fig. 3. The phases T_x , T_y , and NT, previously identified, are also present in the 0-flux configuration. However, the extent of these phases varies from that observed in the ground state sector. Consequently, in the region where $|K_x - K_y| < K_z$ and $K_x + K_y > K_z$, the system is within the topological phase for 0-flux sector, as shown in Fig. 3, and is within the non-topological phase for the ground state sector, as shown in Fig. 2. Hence, by changing the $\{D_j\}$ sector, one can change the topological nature of the model without tuning the parameters.

IV. MAJORANA BOUNDARY MODE

To identify the Majorana zero modes in the topological phase, we review the treatment developed by DeGottardi *et al.* [35]. For given parameters in the topological phase, the Majorana zero modes can be identified as two Majorana operators, $\gamma_A = \sum_j \alpha_j \gamma_{j,A}$ and $\gamma_B = \sum_j \beta_j \gamma_{j,B}$. The double degeneracy of the energy spectrum in the topological phase becomes clear by defining a complex fermion operator, $f = \frac{1}{2}(\gamma_A + i\gamma_B)$, such that $f^\dagger f - 1/2 = \frac{1}{2}i\gamma_A \gamma_B$. Since the f fermion contributes zero energy to the Hamiltonian, the Hamiltonian resides a Z_2 symmetry in the topological phase. The two zero-energy states can be denoted as the eigenstates of the occupation number of f fermion, i.e., $|0\rangle$ and $|1\rangle$. By choosing a particular linear combination of the two states, one simultaneously breaks the Z_2 symmetry and

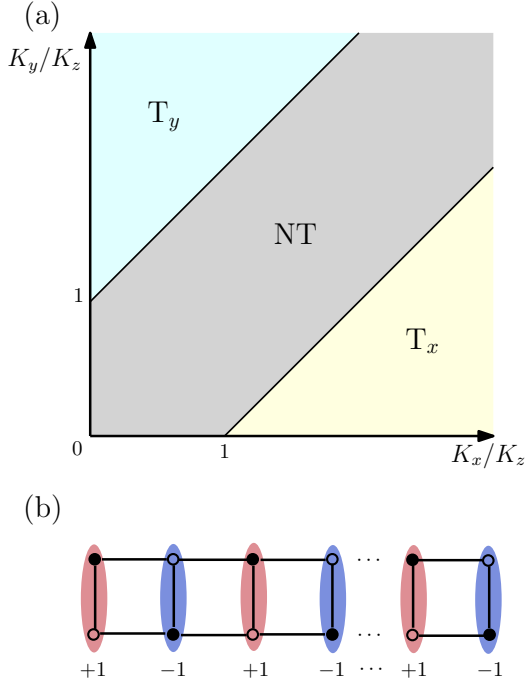


Fig. 2. Fig.(a) and Fig.(b) depict the phase diagram and the corresponding configuration of D_j of the π -flux sector, where $\{D_j\} = \{+1, +1, \dots\}$. T_x and T_y phase are two topological phases with Majorana boundary mode. NT phase represents the non-topological phase.

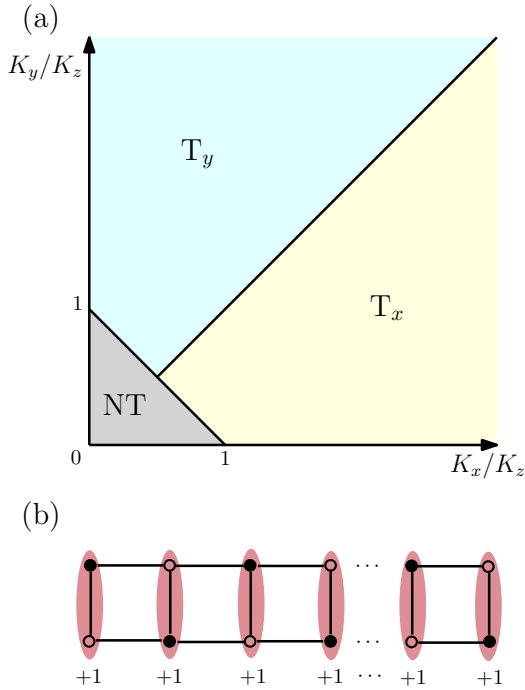


Fig. 3. Fig.(a) and Fig.(b) depict the phase diagram and the corresponding configuration of D_j of the 0-flux sector, where $\{D_j\} = \{+1, +1, \dots\}$. T_x and T_y phase are two topological phases with Majorana boundary mode. NT phase represents the non-topological phase.

determines the expectation values of spin or Majorana operators. To elucidate the relation between Majorana mode and the degenerate states, one consider that the operators, $\{\gamma_A, \gamma_B, i\gamma_A\gamma_B\}$, obey the same commutation relations as the three Pauli matrices. Thus, one can make linear combinations of the state $|0\rangle$ and $|1\rangle$ to construct the eigenbasis, $|\psi_{\pm,A}\rangle$ and $|\psi_{\pm,B}\rangle$, of γ_A and γ_B operator, i.e., $\gamma_A|\psi_{\pm,A}\rangle = \pm|\psi_{\pm,A}\rangle$ and $\gamma_B|\psi_{\pm,B}\rangle = \pm|\psi_{\pm,B}\rangle$. With these basis, it is straightforward to show that $\langle\psi_{\pm,A}|\gamma_{j,A}|\psi_{\pm,A}\rangle = \pm\alpha_j$ and $\langle\psi_{\pm,A}|\gamma_{j,B}|\psi_{\pm,A}\rangle = 0$, with the same for $A \leftrightarrow B$. As a result, the probability of detecting a Majorana fermion at a specific site for the state $|\psi_{\pm,A}\rangle$ is described by the coefficients, $|\alpha_j|^2$ for site (j, A) .

In order to identify the Majorana zero modes, the transfer matrix approach is applied to find the operators γ_A and γ_B . To begin with, one consider the Heisenberg picture with time-dependent operators and time-independent states. The Hamiltonian, Eq. 4, can be considered as a free fermion Hamiltonian with Bogoliubov quasiparticles. For the fermion in the Hamiltonian with energy ω , the time-dependence is described by $f(t) = f(0)e^{-i\omega t}$. For the f -fermion that has the form of $f = \frac{1}{2}(\gamma_A + i\gamma_B)$, the operator γ_A and γ_B also satisfy $\gamma_A(t) = \gamma_A(0)e^{-i\omega t}$ and $\gamma_B(t) = \gamma_B(0)e^{-i\omega t}$. Substitute the form of $\gamma_A(t)$ and $\gamma_B(t)$ into the Heisenberg equation of motion, one obtain the following equations,

$$\begin{aligned} -K_x\gamma_{j-1,B} - K_y\gamma_{j+1,B} + K_zD_j\gamma_{j,B} &= -i\omega\gamma_{j,A}, \\ K_x\gamma_{j+1,A} + K_y\gamma_{j-1,A} - K_zD_j\gamma_{j,A} &= -i\omega\gamma_{j,B}. \end{aligned} \quad (10)$$

Because the Majorana zero modes have zero energy, we look at the $\omega = 0$ case of Eq. 10, which can be solved by real coefficients, α_j and β_j . Combining Eq. 10 with the fact that $\{\gamma_A, \gamma_{j,A}\} = 2\alpha_j$ and $\{\gamma_B, \gamma_{j,B}\} = 2\beta_j$, one can derive the relations of α_j and β_j ,

$$\begin{aligned} -K_x\beta_{j-1} - K_y\beta_{j+1} + K_zD_j\beta_j &= 0, \\ K_x\alpha_{j+1} + K_y\alpha_{j-1} - K_zD_j\alpha_j &= 0. \end{aligned} \quad (11)$$

These coefficients are normalized, ensuring that the edge Majorana operators satisfy $\gamma_A^2 = \gamma_B^2 = 1$. To determine the coefficients of the edge Majorana operators, γ_A and γ_B , one starts with an arbitrary boundary condition, such as $\alpha_1 = 1, \beta_1 = 1$. The remaining coefficients can be determined using Eq. 11.

To elucidate the exponential decay of the probability $|\alpha_j|^2$, we exactly solve Eq. 11 for $\{D_j\} = \{+1, -1, +1, -1, \dots\}$, corresponding to the π -flux sector. From Eq. 11, the relation between β_j is the same as the relation of α_{L-j} for mirror-symmetric $\{D_j\}$. Hence, it is sufficient to exactly solve α_j 's for this case. With

$\{D_j\} = \{+1, -1, +1, -1, \dots\}$, Eq. 11 can be written as

$$\begin{aligned} K_x \alpha_2 + K_z \alpha_1 &= 0, \\ K_x \alpha_3 + K_y \alpha_1 - K_z \alpha_2 &= 0, \\ K_x \alpha_4 + K_y \alpha_2 + K_z \alpha_3 &= 0, \\ K_x \alpha_5 + K_y \alpha_3 - K_z \alpha_4 &= 0, \\ &\vdots \\ K_x \alpha_L + K_y \alpha_{L-2} + (-1)^L \alpha_{L-1} &= 0. \end{aligned} \quad (12)$$

Starting with the boundary condition such that $\alpha_1 = 1$, it follows that $\alpha_2 = -\frac{K_z}{K_x}$. For general integer n , $(\alpha_{2n+1}, \alpha_{2n+2})$ are determined solely by $\alpha_{2n-1}, \alpha_{2n}$, through

$$\begin{aligned} \alpha_{2n+1} &= -\frac{K_y}{K_x} \alpha_{2n-1} + \frac{K_z}{K_x} \alpha_{2n}, \\ \alpha_{2n+2} &= \frac{K_z}{K_x} \frac{K_y}{K_x} \alpha_{2n-1} + \left[-\frac{K_y}{K_x} - \left(\frac{K_z}{K_x} \right)^2 \right] \alpha_{2n}. \end{aligned} \quad (13)$$

We perform linear combinations of these two equations, such that

$$\alpha_{2n+1} + M_{\pm} \alpha_{2n+2} = R_{\pm} (\alpha_{2n-1} + M_{\pm} \alpha_{2n}), \quad (14)$$

where $M_{\pm} = \frac{1}{2K_y} (-K_z \pm \sqrt{K_z^2 + 4K_x K_y})$ and $R_{\pm} = -\frac{K_y}{K_x} + M_{\pm} \left(\frac{K_z}{K_x} \right) \left(\frac{K_y}{K_x} \right)$. Hence, the exact general solution of the coefficients α_j can be obtained from

$$\alpha_{2n+1} + M_{\pm} \alpha_{2n+2} = R_{\pm}^n (\alpha_1 + M_{\pm} \alpha_2). \quad (15)$$

From Eq. 15, it is clear that the linear combinations of the coefficients, α_{2n+1} and α_{2n+2} , exponentially decay or grow as a function of the site index n if and only if $|R_+| > 1$ and $|R_-| > 1$. Hence, a topological invariant, ν , can be defined as

$$\nu = -\text{sgn} [(|R_+| - 1)(|R_-| - 1)], \quad (16)$$

where $\nu = 1$ represent the non-topological phase, and $\nu = -1$ represent the topological phase with edge mode. For $\{D_j\} = \{+1, +1, \dots\}$, the topological invariant has the following form,

$$\nu = -\text{sgn} ((K_y - K_x)^2 - K_z^2). \quad (17)$$

For $|K_y - K_x| > K_z$, the probability of locating Majorana fermion for $|\psi_{+,A/B}\rangle$ is exponentially decaying or growing as a function of the site index j , indicating the edge Majorana mode. For $|K_y - K_x| < K_z$, there is no such exponential decay or growth. Hence, the phase is identified as the non-topological phase, with the quantum phase transition lines confirmed as $|K_y - K_x| = K_z$. These results match with the exact solution for the Majorana fermion model with PBC in Sec. III.

In order to confirm the Majorana zero mode, we perform numerical simulations with fixed flux sectors and open boundary conditions (OBC). The Hamiltonian is

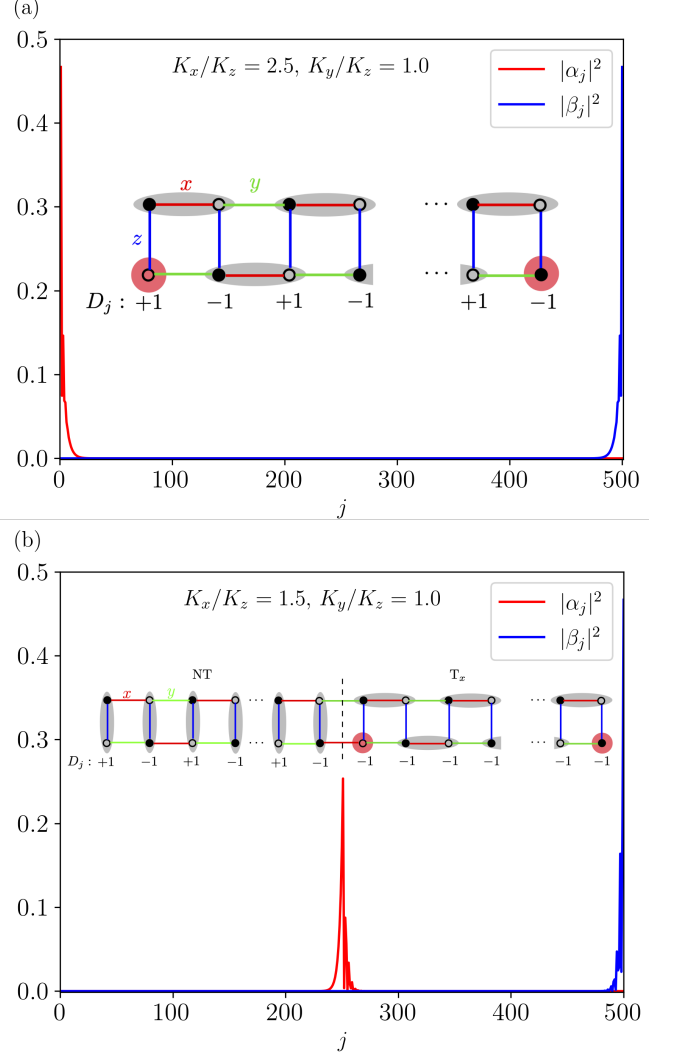


Fig. 4. (a) The coefficients of the Majorana zero modes obtained from diagonalizing the fermion Hamiltonian with $K_x = 2.5$, $K_y = 1.0$, $K_z = 1.0$ and $\{D_j\} = \{+1, -1, +1, -1, \dots\}$. One Majorana zero mode is located at each end of the ladder. The illustration depicts the Majorana fermion correlation in the topological phase, with the red circle indicates isolated Majorana mode. (b) The Majorana zero mode emerges at the interface of the topological phase, T_x , and non-topological phase for the Kitaev ladder system with $K_x = 1.5$, $K_y = 1.0$, $K_z = 1.0$. For j from 1 to $L/2$, D_j is chosen as $(-1)^j$, which is identified as non-topological phase. For j from $L/2 + 1$ to L , $D_j = -1$, which is identified as T_x phase. The illustration depicts the Majorana zero mode located at the interface of two phases, with red circle represents localized Majorana fermion.

represented as $\mathcal{H} = \sum_{j\mu, k\nu} A_{(j\mu, k\nu)} (i\gamma_{j,\mu}\gamma_{k,\nu})$. The quasi-particle excitations are characterized by the linear superposition of Majorana fermions, which is determined by the eigenvectors of the Hermitian matrix $A_{(j\mu, k\nu)}$. In Fig. 4(a), we plot $|\alpha_j|^2$ and $|\beta_j|^2$, which represent the edge Majorana zero modes on each edge of the system using $N = 1000$, i.e., $L = 500$ rungs with $K_x/K_z = 2.5$,

$K_y/K_z = 1.0$, and $\{D_j\} = \{+1, -1, \dots\}$. The red circle in the inset indicates the localized Majorana mode, while the grey oval denotes a stronger x-bond in the $K_x \gg K_y, K_z$ limit, which is in the T_x phase. Note that these coefficients decay exponentially when moving to the bulk of the system, which agrees with the analytically obtained α_j and β_j . In addition to the edge of the system, localized Majorana fermion can also emerge at the interface of topological and non-topological phases. To demonstrate this, we diagonalize $A_{(j\mu, k\nu)}$ for a system size of $L = 500$, with $K_x/K_z = 1.5$, $K_y/K_z = 1.0$. The flux sector is chosen as $\{D_j\} = \{+1, -1, \dots\}$ for j from 1 to $L/2$, and $\{D_j\} = \{-1, -1, \dots\}$ for j from $L/2 + 1$ to L . The dashed line in the inset represents the interface of the topological and non-topological phase. The probability of Majorana fermion locating at each site are plotted in Fig. 4(b). The one Majorana mode, which is represented by the red dot near the dashed line, appears at the interface of the non-topological and the topological phases.

V. MANIPULATION AND FUSION OF MAJORANA MODES

In Sec. III and Sec. IV, we explore the phase diagram and boundary modes for both the π -flux and the 0-flux sector of the Kitaev spin ladder. Notably, for different D_j sectors under identical coupling constants, the phase can be either topological or non-topological. Consequently, the Majorana fermions can be adiabatically transitioned by varying D_j , facilitating the potential for manipulating and fusing of Majorana fermions. In this section, we demonstrate that how the Majorana fermion can be moved and fused in the Kitaev ladder by changing the Z_2 flux.

Here we demonstrate the moving and fusion of Majorana fermions. In order to change the topological nature of the system through changing $\{D_j\}$ configurations, the parameters are chosen to satisfy $|K_x - K_y| < K_z$ and $K_x + K_y > K_z$. The system is initially prepared to be in topological phase (T phase), i.e., either T_x or T_y phase, with $\{D_j\} = \{+1, +1, \dots\}$, which is depicted in Fig. 5(a). In the initial setup, two Majorana fermions, γ_A and γ_B , reside on the edge of the ladder. To move the Majorana fermion, D_j is flipped from $+1$ to -1 on the even number rungs through local spin operations introduced in Sec. II. When $\{D_j\}$ is changed from $\{D_j\} = \{+1, +1, \dots\}$ to $\{D_j\} = \{+1, -1, +1, -1, \dots\}$, the topological nature of that region is changed from T phase to NT phase. The Majorana fermion is then moved adiabatically from the edge of the system to the interface of the NT and T phase, which is illustrated in Fig. 5(b). As γ_A moves further towards the boundary, the two Majorana fermions can fuse into either the vacuum $|0\rangle$ or the complex fermion $f^\dagger|0\rangle$, as illustrated in Fig. 5(c). The two Majorana fermions have interaction through short-range interactions in the Hamiltonian.

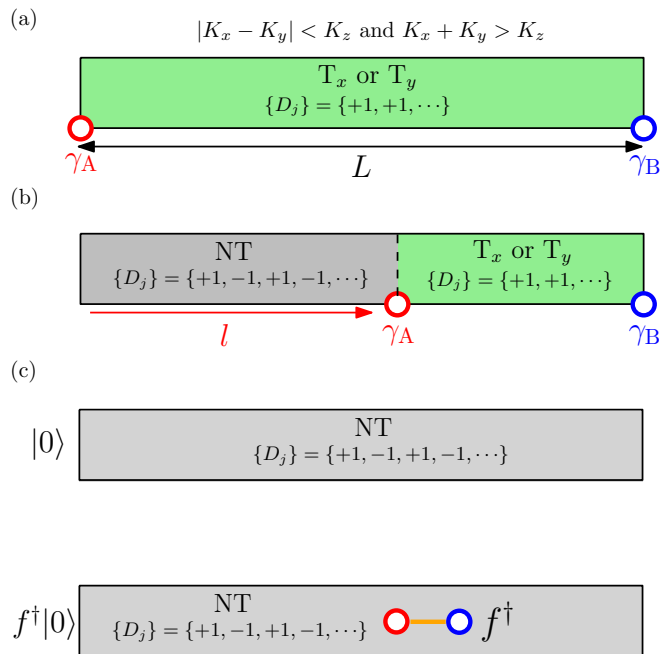


Fig. 5. The illustration of moving Majorana fermion. The interaction strength is set to satisfy $|K_x - K_y| < K_z$. (a) The system is initialized with $\{D_j\} = \{+1, +1, \dots\}$, which gives the topological phase, T_x or T_y , with edge Majorana fermion γ_A and γ_B . (b) The Majorana fermion, γ_A , is moved by spin operations that change the Z_2 flux, D_j . The Z_2 flux configuration is changed to $\{+1, -1, +1, -1, \dots\}$, which turns the gray region from topological phase to the NT phase. The Majorana fermion γ_A is adiabatically moved from the left boundary of the material to the interface of the NT and topological phase. (c) The two resulting state of Majorana fusion. Depending on the initial state in (a), the state after fusion is either vacuum, $|0\rangle$ or a fermion excitation, $f^\dagger|0\rangle$.

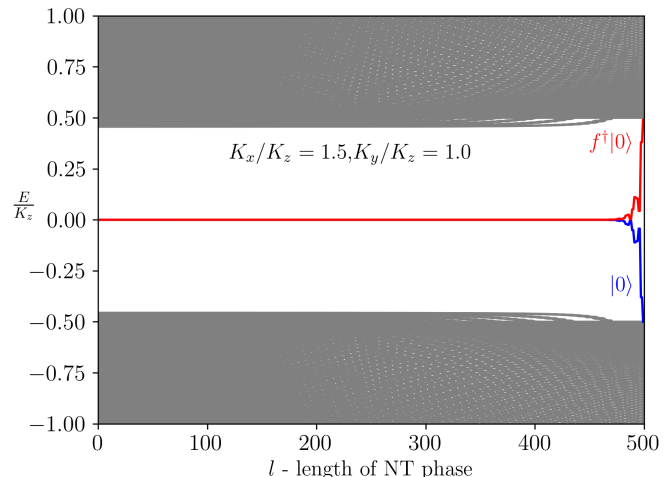


Fig. 6. The numerical simulation of the fusion process depicted in Fig. 5. The energy spectrum for E/K_z from -1 to 1 is plotted. After fusion the state becomes either the ground state or with a fermion excitation, indicated by the blue and red lines.

Numerical simulation is conducted in order to confirm the moving and fusion of Majorana fermions by changing $\{D_j\}$. The Majorana fermion Hamiltonian with OBC is diagonalized with $N = 1000$ sites with fixed parameter choice $(K_x/K_z, K_y/K_z) = (1.5, 1)$. The process depicted in Fig. 5 is simulated numerically. The energy spectrum from $-K_z$ to K_z is plotted as a function of l in Fig. 6, where l denotes the length of the NT phase. We start with $l = 0$, which corresponds to Fig. 5(a), i.e., all the material is within the topological phase. For a finite l , we confirm the existence of the double degeneracy, which is attributed to two isolated Majorana fermions. One of the Majorana fermions resides at the interface of the NT and T phase, while the other Majorana fermion resides on the right edge of the system, as depicted in Fig. 5. When l approaches $L = 500$, the rapid increasing of the energy of the complex fermion is observed. One of the state becomes the ground state, which is represented by the blue line. The other state becomes a complex fermion excitation, $f = \frac{1}{2}(\gamma_A + i\gamma_B)$, which has finite energy in the Hamiltonian.

VI. ENGINEERING A KITAEV SPIN LADDER AND CHALLENGES

In this section we propose how to engineer a Kitaev spin ladder. The Kitaev interaction is originated from the indirect exchange process between $J_{\text{eff}} = 1/2$ wavefunction at the transition metal site and p -orbital at anion sites when they make 90° bond angle.[44] For example, for Ru^{3+} ions with $4d^5$ electron configuration surrounded by Cl^- octahedron, the low energy physics is described by $J_{\text{eff}} = 1/2$, due to a combination of electron correlation and spin-orbital coupling. The bond-dependent Kitaev term is emerged from the interactions between these $J_{\text{eff}} = 1/2$ pseudo-spins via indirect exchange path with p -orbital. In order to get the Kitaev ladder geometry as illustrated in Fig. 7(a), the exchange path towards the adjacent ladders must be frozen. To achieve this, we replace the magnetic $J_{\text{eff}} = 1/2$ ions, for instance RuCl_3 , with non-magnetic ions such as IrCl_3 with filled d^6 ions, except for the two coupled zig-zag chains as shown in Fig. 7(a). To block a possible charge transfer between the magnetic and nonmagnetic ions, a thin insulating barrier may be needed.

Note that Fig. 7(a) is merely an illustration rather than a real crystal structure. The exchange interaction between sites would give us the bond-dependent Kitaev interaction, as well as other interactions. The 1D Kitaev-like term can be realized in this trimmed honeycomb ladder through the nearest-neighbor interaction, $K = (K_x, K_y, K_z)$ as discussed above, but one of the z -bond interactions with a longer distance is replaced by K'_z , as depicted in Fig. 7(b).

Taking into account the alternating z -bond interaction for the trimmed honeycomb ladder, and writing the spin-spin interaction in terms of Majorana fermions, which

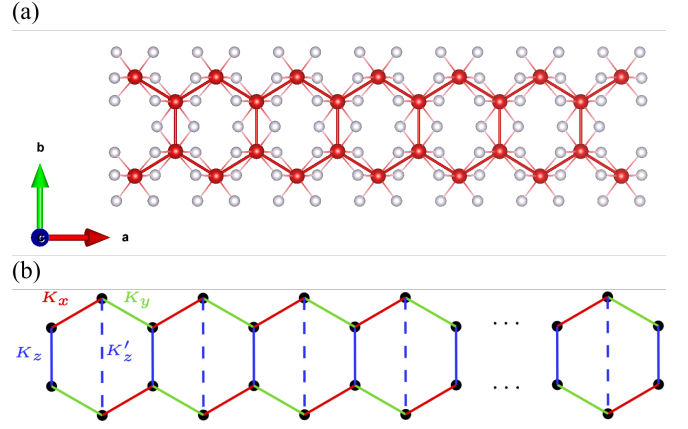


Fig. 7. (a) An illustration of the engineered Kitaev ladder. The red dots represent atoms with $J_{\text{eff}}=1/2$ wavefunction surrounded by p -orbitals of ligand atoms depicted by white dots. The ladder is confined by the insulating barrier. See the main text for details. (b) The trimmed honeycomb ladder geometry with the alternating z -bond interaction. K'_z represents the z -bond with a longer distance.

have the same definition in Sec. II, the Hamiltonian reads:

$$\begin{aligned} \mathcal{H} = & \frac{1}{4} \sum_{j=1}^L [iK_x \gamma_{2j-1,B} \gamma_{2j,A} - iK_y \gamma_{2j-1,A} \gamma_{2j,B} \\ & + K_z (i\gamma_{2j-1,A} \gamma_{2j-1,B}) D_{2j-1} \\ & + iK_x \gamma_{2j,B} \gamma_{2j+1,A} - iK_y \gamma_{2j,A} \gamma_{2j+1,B} \\ & + K'_z (i\gamma_{2j,A} \gamma_{2j,B}) D_{2j}]. \end{aligned} \quad (18)$$

According to Lieb's theorem, the ground state resides in the π -flux sector. In the π -flux sector, the energy dispersion has four bands, $(\epsilon_{k,+}, \epsilon_{k,-}, -\epsilon_{k,+}, -\epsilon_{k,-})$, where

$$\begin{aligned} \epsilon_{\pm,k}^2 = & (K_x + K_y)^2 \cos^2 \frac{k}{2} + (K_x - K_y)^2 \sin^2 \frac{k}{2} \\ & + \frac{1}{2} (K_z^2 + K_z'^2) \\ & \pm \left\{ (K_z - K_z')^2 [(K_y + K_x)^2 + \frac{1}{4} (K_z + K_z')^2] \right. \\ & \left. + 4(K_y K_z - K_x K_z') (K_y K_z' - K_x K_z) \sin^2 \frac{k}{2} \right\}^{\frac{1}{2}}. \end{aligned} \quad (19)$$

The gap is closed at $|K_x - K_y| = \sqrt{K_z K_z'}$. The energy dispersion of the 0-flux sector can be obtained by the transformation $K'_z \rightarrow -K'_z$. The transition lines where the gap closes are $|K_x + K_y| = \sqrt{K_z K_z'}$ and $K_x = K_y (|K_x + K_y| > \sqrt{K_z K_z'})$. The phase diagram of different $\{D_j\}$ sectors of the trimmed ladder model is drawn in Fig. 8. The solid lines demonstrate the transition lines in the ground state sector, $\{D_j\} = \{+1, -1, +1, -1, \dots\}$. The dashed lines represent transition lines in the 0-flux sector, where $\{D_j\} = \{+1, +1, \dots\}$. The blue lines reproduce the same phase diagram as $K_z = K_z'$, while the red lines correspond to the case with $K'_z/K_z = 1/4$. One

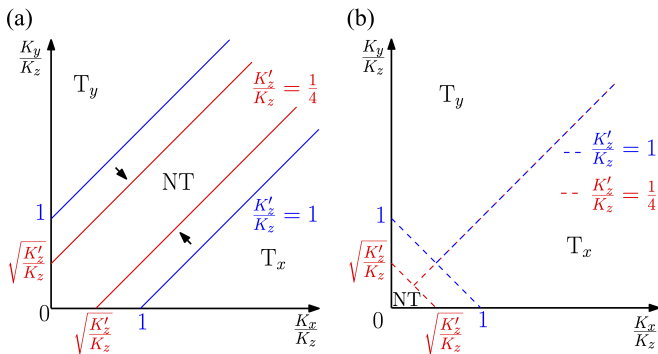


Fig. 8. Phase diagram of the trimmed honeycomb ladder. Blue and red color represent $K'_z = K_z$, the original model studied in previous section, and $K'_z = \frac{1}{4}K_z$, respectively. The black arrows show the change of the transition lines when K'_z/K_z is moving from 1 to a smaller value. (a) Solid lines represent transition line in the ground state sector, $\{D_j\} = \{+1, +1, \dots\}$, i.e., π -flux. (b) Dashed lines represent transition lines in the 0-flux sector, where $\{D_j\} = \{+1, -1, +1, -1, \dots\}$.

can understand the phase diagram by moving from the $K'_z/K_z = 1$ case to $K'_z < K_z$ case, the phase transition lines are shifted as the black arrows indicate. When $K'_z \rightarrow 0$, the two lines in both π -flux and 0-flux merge to one line. At that limit, the energy dispersion goes to $\epsilon_{\pm,k} = \sqrt{(K_x + K_y)^2 - 4K_x K_y \sin^2 \frac{k}{2} + K_z^2/4} \pm K_z/2$. The transition line is $K_x = K_y$. In this limit, there exists macroscopic number of zero modes. Because the z -bonds for even number of rungs are missing, the Z_2 flux at the missing rungs, $i\tilde{\gamma}_{2j,A}\tilde{\gamma}_{2j,B}$, have zero energy in the Hamiltonian, resulting in $2^{L/2}$ -fold degeneracy. The region which is within the two solid lines are of interest, as the model is non-topological in the π -flux sector and is topological in the 0-flux sector. The square root dependence guarantees that even for small K'_z/K_z , for instance, $K'_z/K_z = 0.01$, the region still has a noticeable width of 0.1 in the phase diagram.

Note that the engineering of such a material is primarily theoretical in nature. This is because, in order to prevent other symmetry-allowed interactions among $J_{\text{eff}} = 1/2$ pseudospins, such as Heisenberg and Γ interactions [12, 45], one must inhibit direct exchange processes, a task that presents significant challenges. Additionally, it is highly probable that the ideal octahedral structure is modified due to the presence of an insulating barrier along the ladder. This would introduce additional interactions which further spoil the exactly solvable problem. Additionally, while it has been established that the extended Kitaev ladder model exhibits the same Kitaev phase as the Kitaev point, albeit with small Heisenberg and Γ interactions [39, 40, 44, 45], the identification of Majorana edge modes beyond the exact solvable point remains a question. We defer these inquiries to future studies.

VII. SUMMARY AND DISCUSSION

Identifying and manipulating fractionalized excitations that encode non-Abelian statistics in many body systems is essential for realizing TQC. Examples of systems exhibiting fractionalized excitations and non-Abelian statistics include $p + ip$ superconductor and the Kitaev spin model. Meanwhile, studies are also focused on 1D p -wave superconductors, which host edge Majorana mode in the topological phase. The isolated Majorana modes in wire networks are proposed to encode non-Abelian statistics. These studies demonstrate the potential realization of TQC using 1D topological systems.

Motivated by research into 1D p -wave superconductivity and the Kitaev spin model, we investigate the spin-1/2 Kitaev ladder systems. The spin-1/2 ladder can be conceptualized by Majorana fermions coupled with Z_2 flux D_j defined on a vertical bond j . The ground state has $\{D_j\} = \{+1, -1, \dots\}$ and $\{-1, 1, \dots\}$, which are degenerate. We first found the projective measurement that selects one of the ground states. Once the state is selected, we can apply the local spin operators on a bond, such as $\sigma_j^x \sigma_{j+1}^x$ on a y -bond, which flips the sign of the adjacent D_j and D_{j+1} . Repeating such operators enables the system to reach a desired Z_2 flux configuration.

We then show the phase diagrams with the π -flux and 0-flux sector, which contain different phase transition lines. By manipulating the Z_2 flux sector through local spin operators as discussed above, the topological nature of the system can be manipulated with given parameters. Isolated Majorana modes are identified through analytical and numerical techniques at both the edge of the topological phase and the interface between topological and non-topological phase. We investigate the process of moving and fusion of the Majorana zero modes by changing the Z_2 flux. When the Majorana mode at the interface between non-topological and topological phases moves, via the sign change of D_j , toward the end of the topological phase boundary, the two Majorana modes become a vacuum or a complex fermion depending on the initial state.

Furthermore, we explore the engineering principles behind creating a Kitaev spin ladder. Given that the Kitaev honeycomb structure is constructed by coupling zig-zag Kitaev chains, the ladder could be actualized by replacing $J_{\text{eff}} = 1/2$ ions such as RuCl_3 with those possessing a filled shell configuration, such as IrCl_3 with d^6 , except for two chains. To prevent any charge transfer, a thin insulating barrier may be required. We derive the phase diagram for this trimmed honeycomb ladder and confirm the persistence of Majorana modes found in the regular ladder. Consequently, our method of manipulating Majorana fermions remains applicable to an alternative z -bond due to the geometry of the trimmed honeycomb ladder. The current study is predominantly theoretical, and we address the challenges associated with such engineering, including symmetry-allowed interactions and potential deformation of the octahedral structure. De-

spite these challenges, we hope that our protocol could be realized in the future.

ACKNOWLEDGEMENT

This work is supported by the Natural Sciences and Engineering Research Council of Canada (NSERC) Discovery Grant No. 2022-04601. H.Y.K acknowledges the

support by the Canadian Institute for Advanced Research (CIFAR) and the Canada Research Chairs Program. Computations were performed on the Niagara supercomputer at the SciNet HPC Consortium. SciNet is funded by: the Canada Foundation for Innovation under the auspices of Compute Canada; the Government of Ontario; Ontario Research Fund - Research Excellence; and the University of Toronto.

-
- [1] A. Kitaev, Fault-tolerant quantum computation by anyons, *Annals of Physics* **303**, 2 (2003).
- [2] M. H. Freedman, P/np, and the quantum field computer, *Proceedings of the National Academy of Sciences* **95**, 98 (1998).
- [3] S. Das Sarma, M. Freedman, and C. Nayak, Topologically protected qubits from a possible non-abelian fractional quantum hall state, *Phys. Rev. Lett.* **94**, 166802 (2005).
- [4] C. Nayak, S. H. Simon, A. Stern, M. Freedman, and S. Das Sarma, Non-abelian anyons and topological quantum computation, *Rev. Mod. Phys.* **80**, 1083 (2008).
- [5] M. Freedman, A. Kitaev, M. Larsen, and Z. Wang, Topological quantum computation, *Bulletin of the American Mathematical Society* **40**, 31 (2003).
- [6] A. Stern and N. H. Lindner, Topological quantum computation—from basic concepts to first experiments, *Science* **339**, 1179 (2013).
- [7] G. Volovik, Fermion zero modes on vortices in chiral superconductors, *Journal of Experimental and Theoretical Physics Letters* **70**, 609 (1999).
- [8] D. A. Ivanov, Non-abelian statistics of half-quantum vortices in p -wave superconductors, *Phys. Rev. Lett.* **86**, 268 (2001).
- [9] L. Fu and C. L. Kane, Superconducting proximity effect and majorana fermions at the surface of a topological insulator, *Phys. Rev. Lett.* **100**, 096407 (2008).
- [10] A. Kitaev, Anyons in an exactly solved model and beyond, *Annals of Physics* **321**, 2 (2006), january Special Issue.
- [11] W. Witczak-Krempa, G. Chen, Y. B. Kim, and L. Balents, Correlated quantum phenomena in the strong spin-orbit regime, *Annu. Rev. Condens. Matter Phys.* **5**, 57 (2014).
- [12] I. Rousochatzakis, N. B. Perkins, Q. Luo, and H.-Y. Kee, Beyond kitaev physics in strong spin-orbit coupled magnets, *Reports on Progress in Physics* **87**, 026502 (2024).
- [13] J. G. Rau, E. K.-H. Lee, and H.-Y. Kee, Spin-orbit physics giving rise to novel phases in correlated systems: Iridates and related materials, *Annual Review of Condensed Matter Physics* **7**, 195 (2016).
- [14] S. M. Winter, Y. Li, H. O. Jeschke, and R. Valentí, Challenges in design of kitaev materials: Magnetic interactions from competing energy scales, *Phys. Rev. B* **93**, 214431 (2016).
- [15] S. M. Winter, A. A. Tsirlin, M. Daghofer, J. van den Brink, Y. Singh, P. Gegenwart, and R. Valentí, Models and materials for generalized kitaev magnetism, *Journal of Physics: Condensed Matter* **29**, 493002 (2017).
- [16] M. Hermanns, I. Kimchi, and J. Knolle, Physics of the kitaev model: fractionalization, dynamic correlations, and material connections, *Annual Review of Condensed Matter Physics* **9**, 17 (2018).
- [17] H. Takagi, T. Takayama, G. Jackeli, G. Khaliullin, and S. E. Nagler, Concept and realization of kitaev quantum spin liquids, *Nature Reviews Physics* **1**, 264 (2019).
- [18] Y. Motome and J. Nasu, Hunting majorana fermions in kitaev magnets, *Journal of the Physical Society of Japan* **89**, 012002 (2020).
- [19] T. Takayama, J. Chaloupka, A. Smerald, G. Khaliullin, and H. Takagi, Spin-orbit-entangled electronic phases in 4d and 5d transition-metal compounds, *Journal of the Physical Society of Japan* **90**, 062001 (2021).
- [20] S. Trebst and C. Hickey, Kitaev materials, *Physics Reports* **950**, 1 (2022), kitaev materials.
- [21] M. Sato and Y. Ando, Topological superconductors: a review, *Reports on Progress in Physics* **80**, 076501 (2017).
- [22] C. Beenakker, Search for majorana fermions in superconductors, *Annual Review of Condensed Matter Physics* **4**, 113 (2013).
- [23] J. Alicea, New directions in the pursuit of majorana fermions in solid state systems, *Reports on Progress in Physics* **75**, 076501 (2012).
- [24] M. Leijnse and K. Flensberg, Introduction to topological superconductivity and majorana fermions, *Semiconductor Science and Technology* **27**, 124003 (2012).
- [25] T. D. Stanescu and S. Tewari, Majorana fermions in semiconductor nanowires: fundamentals, modeling, and experiment, *Journal of Physics: Condensed Matter* **25**, 233201 (2013).
- [26] S. R. Elliott and M. Franz, Colloquium: Majorana fermions in nuclear, particle, and solid-state physics, *Rev. Mod. Phys.* **87**, 137 (2015).
- [27] S. D. Sarma, M. Freedman, and C. Nayak, Majorana zero modes and topological quantum computation, *npj Quantum Information* **1**, 1 (2015).
- [28] S. Frolov, M. Manfra, and J. Sau, Topological superconductivity in hybrid devices, *Nature Physics* **16**, 718 (2020).
- [29] X.-L. Qi and S.-C. Zhang, Topological insulators and superconductors, *Rev. Mod. Phys.* **83**, 1057 (2011).
- [30] D. Aasen, M. Hell, R. V. Mishmash, A. Higginbotham, J. Danon, M. Leijnse, T. S. Jespersen, J. A. Folk, C. M. Marcus, K. Flensberg, and J. Alicea, Milestones toward majorana-based quantum computing, *Phys. Rev. X* **6**, 031016 (2016).
- [31] J. Alicea, Y. Oreg, G. Refael, F. Von Oppen, and M. P. Fisher, Non-abelian statistics and topological quantum information processing in 1d wire networks, *Nature Physics* **7**, 412 (2011).

- [32] J. Bai, Q. Wang, L. Xu, W. Feng, and X.-Q. Li, Probing the non-abelian fusion of a pair of majorana zero modes, *Phys. Rev. B* **109**, 085403 (2024).
- [33] B. Van Heck, A. Akhmerov, F. Hassler, M. Burrello, and C. Beenakker, Coulomb-assisted braiding of majorana fermions in a josephson junction array, *New Journal of Physics* **14**, 035019 (2012).
- [34] X.-Y. Feng, G.-M. Zhang, and T. Xiang, Topological characterization of quantum phase transitions in a spin-1/2 model, *Phys. Rev. Lett.* **98**, 087204 (2007).
- [35] W. DeGottardi, D. Sen, and S. Vishveshwara, Topological phases, majorana modes and quench dynamics in a spin ladder system, *New Journal of Physics* **13**, 065028 (2011).
- [36] H.-D. Chen and Z. Nussinov, Exact results of the kitaev model on a hexagonal lattice: spin states, string and brane correlators, and anyonic excitations, *Journal of Physics A: Mathematical and Theoretical* **41**, 075001 (2008).
- [37] A. Catuneanu, E. S. Sørensen, and H.-Y. Kee, Nonlocal string order parameter in the $s = \frac{1}{2}$ kitaev-heisenberg ladder, *Phys. Rev. B* **99**, 195112 (2019).
- [38] C. E. Agrapidis, J. van den Brink, and S. Nishimoto, Ground state and low-energy excitations of the kitaev-heisenberg two-leg ladder, *Phys. Rev. B* **99**, 224418 (2019).
- [39] E. S. Sørensen, A. Catuneanu, J. S. Gordon, and H.-Y. Kee, Heart of entanglement: Chiral, nematic, and incommensurate phases in the kitaev-gamma ladder in a field, *Phys. Rev. X* **11**, 011013 (2021).
- [40] E. S. Sørensen and H.-Y. Kee, Twice hidden string order and competing phases in the spin-1/2 kitaev-gamma ladder, *npj Quantum Materials* **9**, 10 (2024).
- [41] Y. Chen, Y.-C. He, and A. Szasz, Phase diagrams of spin- s kitaev ladders, *Phys. Rev. B* **108**, 045124 (2023).
- [42] A. Langari, A. Mohammad-Aghaei, and R. Haghshenas, Quantum phase transition as an interplay of kitaev and ising interactions, *Phys. Rev. B* **91**, 024415 (2015).
- [43] E. H. Lieb, Flux phase of the half-filled band, *Phys. Rev. Lett.* **73**, 2158 (1994).
- [44] G. Jackeli and G. Khaliullin, Mott insulators in the strong spin-orbit coupling limit: From heisenberg to a quantum compass and kitaev models, *Phys. Rev. Lett.* **102**, 017205 (2009).
- [45] J. G. Rau, E. K.-H. Lee, and H.-Y. Kee, Generic spin model for the honeycomb iridates beyond the kitaev limit, *Phys. Rev. Lett.* **112**, 077204 (2014).

Appendix A: Ground states in extreme limit

In order to understand the double degeneracy of the ground states, we perform perturbation theory studies. We consider the limit when $K_z \gg K_x, K_y$. The Hamiltonian is

$$\mathcal{H} = H_0 + V, \quad (\text{A1})$$

where $H_0 = \frac{K_z}{4} \sum_{\langle j,k \rangle \in z\text{-bond}} \sigma_j^z \sigma_k^z$ and $V = \frac{K_x}{4} \sum_{\langle j,k \rangle \in x\text{-bond}} \sigma_j^x \sigma_k^x + \frac{K_y}{4} \sum_{\langle j,k \rangle \in y\text{-bond}} \sigma_j^y \sigma_k^y$. We relabel the site as depicted in Fig. 9. In the zeroth order, there is only z -bond Ising interactions. In each

vertical bond of the ladder, the quantum state is either $|\uparrow\downarrow\rangle_{2j-1,2j}$ or $|\downarrow\uparrow\rangle_{2j-1,2j}$, while the states with the same spin alignment, $|\uparrow\uparrow\rangle_{2j-1,2j}$ and $|\downarrow\downarrow\rangle_{2j-1,2j}$, have the energy $\sim K_z$, which is a much higher energy that we ignore for the construction of the effective Hamiltonian. We denote $|\uparrow\rangle_j = |\uparrow\downarrow\rangle_{2j-1,2j}$ and $|\downarrow\rangle_j = |\downarrow\uparrow\rangle_{2j-1,2j}$. With these two basis, one can construct the $SU(2)$ algebra with three Pauli matrices, defined as

$$\begin{aligned} \tau_j^x &= |\uparrow\rangle_j \langle \downarrow_j| + |\downarrow\rangle_j \langle \uparrow_j|, \\ \tau_j^y &= -i |\uparrow\rangle_j \langle \downarrow_j| + i |\downarrow\rangle_j \langle \uparrow_j|, \\ \tau_j^z &= |\uparrow\rangle_j \langle \uparrow_j| - |\downarrow\rangle_j \langle \downarrow_j|. \end{aligned} \quad (\text{A2})$$

According to perturbation theory, which is reviewed in [10], the effective Hamiltonian has the form of

$$H_{\text{eff}} = \Pi_0^\dagger (V + V G'_0(E_0) V + V G'_0(E_0) V G'_0(E_0) V + \dots) \Pi_0, \quad (\text{A3})$$

where Π_0 is the projector onto the ground state subspace, $G'_0(E_0) = ((E_0 - H_0)^{-1})'$ is the Green's function that only acts on the excited states and vanishes when acting on ground states. For the first order, we have $H_{\text{eff}}^{(1)} = 0$. The first non-vanishing order is the second order, the second order effective Hamiltonian is

$$H_{\text{eff}}^{(2)} = -\frac{K_x K_y}{4K_z} \sum_j \tau_j^x \tau_{j+1}^y, \quad (\text{A4})$$

which is the Ising model along τ^y axis. Hence, there exists two fold degenerate ground states, $|\psi_1\rangle$ and $|\psi_2\rangle$, defined as

$$\begin{aligned} |\psi_1\rangle &= |+_y, +_y, \dots, +_y\rangle = |+_y\rangle_1 |+_y\rangle_2 \dots |+_y\rangle_L, \\ |\psi_2\rangle &= |-_y, -_y, \dots, -_y\rangle = |-_y\rangle_1 |-_y\rangle_2 \dots |-_y\rangle_L, \end{aligned} \quad (\text{A5})$$

where $|\pm_y\rangle_j = |\uparrow\rangle_j \pm i |\downarrow\rangle_j$ are two eigenstates of the τ_j^y operator. These two states are related through time reversal symmetry, i.e., $T|\psi_1\rangle = |\psi_2\rangle$ and vice versa. To see the relation between these two states and $\{D_j\}$ sectors, we express the D_j operators using τ operators when effectively acting on the ground state subspace,

$$D_j = (-1)^{j+1} \tau_j^x \prod_{k \neq j} \tau_k^z. \quad (\text{A6})$$

It is straightforward to check that $D_j |\psi_1\rangle = (-1)^{j+1} i |\psi_2\rangle$ and $D_j |\psi_2\rangle = (-1)^{j+1} (-i) |\psi_1\rangle$. Hence, the two-fold degeneracy can be characterized by the two $\{D_j\}$ sectors,

$$\begin{aligned} |\psi_1\rangle + i |\psi_2\rangle &\text{ with } \{D_j\} = \{+1, -1, +1, -1, \dots\}, \\ |\psi_1\rangle - i |\psi_2\rangle &\text{ with } \{D_j\} = \{-1, +1, -1, +1, \dots\}. \end{aligned} \quad (\text{A7})$$

Appendix B: Methods of applying spin operators through magnetic field

In order to change D_j values, local spin operators, for instance, $\sigma_j^x \sigma_k^x$ on y -bond, is needed to be applied on the

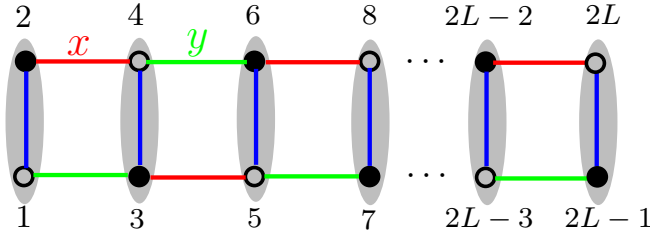


Fig. 9. Applying perturbation theory in the limit with $K_z \gg K_x, K_y$. The gray shade indicates that K_z interaction is dominant.

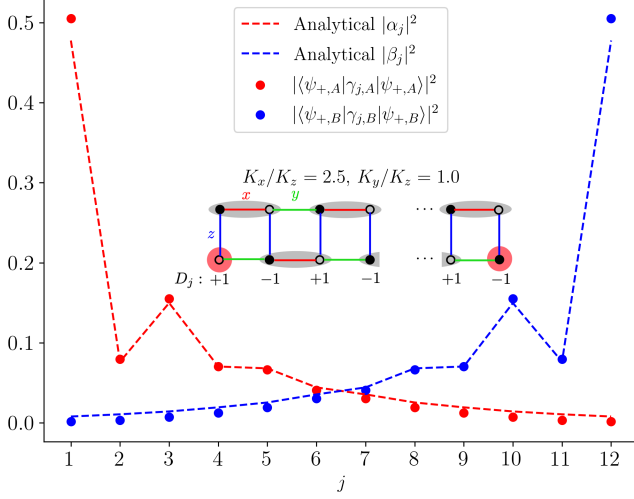


Fig. 10. ED calculation with 24 spin sites with fixed $\{D_j\}$ sector. The blue and red dot represents the expectation value of Majorana fermion for $|\psi_{+,A}\rangle$ and $|\psi_{-,B}\rangle$, which are linear combination of the two lowest energy states. The dashed line represents the analytical coefficients α_j and β_j derived from Sec. IV. The deviation comes from finite size effect.

spin system. The local spin operator could be applied through applying a magnetic field on a bond for a short time of δt . To understand the process, let us consider the Hamiltonian $H = \mathcal{H}_K + \mathcal{H}_B$, where

$$\mathcal{H}_B = \frac{\mu_B B \hbar}{2} (\sigma_j^x + \sigma_k^x) [\theta(t - t_0) - \theta(t - (t_0 + \delta t))], \quad (\text{B1})$$

where \mathcal{H}_K is the Hamiltonian for the Kitaev spin ladder, j, k belongs to y -bond that connect nearby D_j , $\theta(t)$ is the step function with $\theta(t) = 0$ for $t < 0$ and $\theta(t) = 1$ for

$t > 0$. When considering the time evolution of the state with Schrödinger equation, the state evolves from t_0 to $t_0 + \delta t$ as

$$|\psi(t_0 + \delta t)\rangle = e^{-i(\mathcal{H}_K + \mathcal{H}_B)\delta t/\hbar} |\psi(t_0)\rangle. \quad (\text{B2})$$

In order to prevent the system to enter another phase, δt need to be controlled to satisfy $\frac{E\delta t}{\hbar} \ll 1$, where E is the energy of the state. With these approximation, the time evolution can be approximated by

$$|\psi(t_0 + \delta t)\rangle \simeq e^{-i\mathcal{H}_B\delta t/\hbar} |\psi(t_0)\rangle. \quad (\text{B3})$$

Hence, to effectively apply the operator $\sigma_j^x \sigma_k^x$, the magnetic field should satisfy

$$\frac{\mu_B B \delta t}{2} = \frac{\pi}{2}, \quad (\text{B4})$$

such that $e^{(-i\sigma^x \pi/2)} = -i\sigma^x$.

Hence, by applying a strong magnetic field with a short period of time on a local bond, one can effectively apply the local spin operator to change the D_j sector. Although the topological nature of the Hamiltonian can be changed through applying these local spin operators, the dynamics of the quantum state needs to be further studied.

Appendix C: ED calculation

In order to confirm the Majorana zero mode in the spin state, we perform exact diagonalization(ED) simulations on the Kitaev ladder spin model using 24 sites for the spin states with $\{D_j\} = \{+1, -1, \dots\}$. Since we are using the open boundary condition, there are four degenerate states. However, since we have fixed one of the two Z_2 flux configurations, there are two degenerate states which represent two edge states with zero energy. The probability of detecting localized Majorana fermion is depicted in Fig. 10 for $|\psi_{+,A}\rangle$ and $|\psi_{+,B}\rangle$, where $|\psi_{+,A}\rangle$ and $|\psi_{+,B}\rangle$ are obtained from the linear combination of nearly-degenerate ground states that maximize the expectation value of γ_A and γ_B operators, respectively. The analytical result is depicted as dashed line for comparison in Fig. 10. Due to the finite size effect, the degeneracy is not perfect, and there is some tiny difference between the analytical result and the numerical calculation. However one can observe qualitatively the Majorana edge mode, even for the small system size.